The Extra-domain A of Fibronectin Is a Vascular Marker of Solid Tumors and Metastases

Jascha-N. Rybak,[1] Christoph Roesli,[1] Manuela Kaspar,[2] Alessandra Villa,[2] and Dario Neri[1]

[1]Department of Chemistry and Applied Biosciences, ETH Zurich, and [2]Philochem AG, c/o ETH Zurich, Zurich, Switzerland

Abstract

One of the most promising new avenues for the development of more selective and efficacious cancer therapies relies on the antibody-mediated targeted delivery of bioactive agents (e.g., cytokines) to the tumor environment. The identification of quantitative differences in the expression of accessible vascular proteins in metastatic lesions and host organs facilitate the development of antibody-based strategies, which should be highly efficient and selective, considering the fact that an over-exuberant neovasculature is a characteristic feature of aggressive cancers, and that tumor blood vessels are readily accessible for i.v. administered therapeutic agents. Metastasis is the main cause of death in cancer. The availability of metastasis-specific antigens accessible from the bloodstream will allow a selective delivery of therapeutic agents to metastatic lesions using antibodies as vehicles. Using a combination of vascular biotinylation of 129Sv mice bearing F9 liver metastases and mass spectrometry, we have identified 435 accessible proteins in metastasis and host organ specimens, of which 117 were exclusively detected in metastases. In particular, we found that the alternatively spliced extra-domain A (EDA) of fibronectin is strongly expressed in the neovasculature of liver metastases, while being undetectable in most normal organs. A human antibody to EDA was used to show EDA expression in the neovasculature of metastases and primary tumors of human cancer patients and to target mouse liver metastases and subcutaneous tumors *in vivo*. Human antibody fragments specific to the EDA domain of fibronectin promise to serve as general vehicles for the efficient and selective delivery of imaging agents or therapeutic molecules to metastatic sites. [Cancer Res 2007;67(22):10948–57]

Introduction

The majority of cancer-related deaths are caused by the metastatic spread of the disease (1). Although a large area of modern anticancer research focuses on the identification and inhibition of gene products that are essential for the metastatic spread of the disease, an equally attractive therapeutic option relies on the antibody-based targeted delivery of bioactive agents [full immunoglobulin Gs (IgG) for Fc-mediated cell killing, drugs, radionuclides, cytokines, photosensitizers, pro-coagulant agents, etc.] to the tumor environment and to metastatic lesions (2–4). In this context, the targeted delivery of bioactive agents to the tumoral neovasculature seems to be a particularly promising anticancer therapeutic modality, in light of the fact that a vigorous neovasculature development is a characteristic feature of both aggressive primary tumors and metastases, and that tumor blood vessels are readily accessible for i.v. administered therapeutic agents (5–7).

Biomedical interventions that target the neovasculature of metastatic cancer crucially rely on the identification of proteins, which are abundantly expressed around the tumor blood vessels while being undetectable in most normal organs and in plasma. A number of experimental strategies have recently been proposed for the identification of vascular tumor markers. They include the transcriptomic analysis of tumor-derived endothelial cells (e.g., ref. 8), bioinformatics strategies that compare gene expression in tumoral and normal endothelial cells (e.g., ref. 9), isolation of antibodies against tumor endothelial cell antigens (e.g., ref. 10), as well as proteomic approaches based on the terminal perfusion of tumor-bearing rats with silica beads, followed by mass spectrometry (MS)–based analysis of proteins stripped from the vascular membranes (11). Only few markers of tumor angiogenesis have been extensively characterized and validated thus far (5, 7, 12). However, our group has developed human monoclonal antibodies capable of vascular targeting in animal models of cancer (for a recent review, see ref. 7) and in patients with solid tumors (13). Two of these products are currently being investigated in phase II clinical trials (14).

We have recently developed a general methodology for the identification of accessible vascular proteins in normal organs and in tumors. This technology relies on the *in vivo* perfusion of tumor-bearing animals (15) or *ex vivo* perfusion of surgically resected human organs with cancer (12), with reactive ester derivatives of biotin, which covalently modify accessible proteins in vascular structures. Biotinylated proteins in different organs can be purified on streptavidin resins, followed by a MS–based identification and relative quantification using liquid chromatography (LC)-MS and LC-MS/MS procedures (16, 17).

In this article, we report a comparative analysis of accessible vascular proteins in mouse liver metastases and in normal liver, obtained by terminal perfusion of mice bearing metastatic F9 tumors (18) with a sulfo-*N*-hydroxysuccinimido ester derivative of biotin. The MS-based analysis of biotinylated proteins recovered from normal liver and from metastatic lesions, followed by immunohistochemical validation of the most promising candidates, revealed striking differences in the expression of several proteins and/or splice variants. In particular, the observation that the alternatively spliced extra-domain A (EDA) and extra-domain B (EDB) domains of fibronectin represent good-quality vascular markers of liver metastases may open novel imaging opportunities and targeted therapeutic modalities.

Note: Supplementary data for this article are available at Cancer Research Online (http://cancerres.aacrjournals.org/).

J.-N. Rybak and C. Roesli contributed equally to the work.

Dario Neri is a founder and shareholder of Philochem AG, a company that holds certain patents related to anti–extra-domain A antibodies.

Requests for reprints: Dario Neri, ETH Zurich, Institute of Pharmaceutical Sciences, Wolfgang-Pauli-Strasse 10, HCI G396, 8093 Zurich, Switzerland. E-mail: dario.neri@pharma.ethz.ch.

doi:10.1158/0008-5472.CAN-07-1436

Materials and Methods

Animal model. Animal experiments were approved by the Swiss Federal Veterinary Office and done in accordance with the Swiss Animal Protection Ordinance. Male 129Sv mice (Charles River Laboratories) received i.v. injection of $\sim 5 \times 10^5$ mutant F9 murine teratocarcinoma cells (18), which had been kindly provided by Dario Rusciano (SIFI, Catania, Italy). Mice were used 3 weeks after tumor cell injection for *in vivo* biotinylation, targeting experiments or organ excision for immunohistochemistry.

***In vivo* biotinylation.** *In vivo* biotinylation experiments were done as described previously (15, 16). A brief description is provided in the Supplementary Experimental Procedures.

After perfusion, organs and tumors were excised, and specimens were either freshly snap-frozen for preparation of organ homogenates or embedded in cryoembedding compound (Microm) and frozen in isopentane in liquid nitrogen for the preparation of cryosections for histochemical analysis. Unperfused mice were used as negative controls for the proteomic analysis.

Preparation of protein extracts for proteomic analysis. Specimens were resuspended in 40 μL/mg tissue of lysis buffer [2% SDS, 50 mmol/L Tris, 10 mmol/L EDTA, CompleteE proteinase inhibitor cocktail (Roche Diagnostics) in PBS (pH 7.4)] and homogenized using an Ultra-Turrax T8 disperser (IKA-Werke). Homogenates were sonicated using a Vibra-cell (Sonics), followed by 15 min incubation at 99°C and 20 min centrifugation at 15,000 × *g*. The supernatant was used as total protein extract. Protein concentration was determined using the BCA Protein Assay Reagent Kit (Pierce).

Purification of biotinylated proteins. For each sample, 960 μL streptavidin-sepharose (Amersham Biosciences) slurry were washed thrice in buffer A (1% NP40, 0.1% SDS in PBS), pelleted, and mixed with 15 mg of total protein extract. Capture of biotinylated proteins was allowed to proceed for 2 h at room temperature in a revolving mixer. The supernatant was removed, and the resin was washed thrice with buffer A, twice with buffer B (0.1% NP40, 1 mol/L NaCl in PBS), and once with 50 mmol/L ammonium bicarbonate. Finally, the resin was resuspended in 400 μL of a 50-mmol/L solution of ammonium bicarbonate and 20 μL of sequencing grade modified porcine trypsin (stock solution of 40 ng/μL in 50 mmol/L ammonium bicarbonate; Promega) were added. Protease digestion was carried out overnight at 37°C under constant agitation. Peptides were desalted, purified, and concentrated with C18 microcolumns (ZipTip C18, Millipore). After lyophilization, peptides were stored at −20°C.

Nanocapillary HPLC with automated online fraction spotting onto matrix-assisted laser desorption/ionization target plates. Tryptic peptides were separated by reverse-phase high-performance liquid chromatography (RP-HPLC) using an UltiMate nanoscale LC system and a FAMOS microautosampler (LC Packings) controlled by the Chromeleon software (Dionex). Mobile phase A consisted of 2% acetonitrile and 0.1% trifluoroacetic acid (TFA) in water, and mobile phase B was 80% acetonitrile and 0.1% TFA in water. The flow rate was 300 nL/min. Lyophilized peptides derived from the digestion of biotinylated protein affinity purified from 1.5 mg of total protein were dissolved in 5 μL of buffer A and loaded on the column (inner diameter, 75 μm; length, 15 cm; filled with C18 PepMap 100, 3-μm, 100-Å beads; LC Packings). The peptides were eluted with a gradient of 0% to 30% B for 7 min, 30% to 80% B for 67 min, 80% to 100% B for 3 min, and 100% B for 5 min; the column was equilibrated with 100% A for 20 min before analyzing the next sample. Eluting fractions were mixed with a solution of 3 mg/mL α-cyano-4-hydroxycinnamic acid, 277 pmol/mL neurotensin (internal standard), 0.1% TFA, and 70% acetonitrile in water and deposed on a 192-well matrix-assisted laser desorption/ionization (MALDI) target plate using an online Probot system (Dionex). The flow of the MALDI-matrix solution was set to 1.083 μL/min. Thus, each fraction collected during 20 s contained 361 nL MALDI-matrix solution and 100 nL sample. The end concentration of neurotensin was 100 fmol per well.

MALDI-TOF/TOF mass spectrometry. MALDI–time-of-flight (TOF) and MALDI-TOF/TOF mass spectrometric analyses were carried out using the 4700 Proteomics Analyzer (Applied Biosystems). A detailed description of the procedure and settings is provided in the Supplementary Experimental Procedures.

Antibodies. Polyclonal goat anti-CD98 (sc-7094) and rat monoclonal anti-perlecan (sc-33707) antibodies were purchased from Santa Cruz Biotechnology. According to information from the provider, the anti-CD98 antibody was raised against a COOH-terminal peptide from the CD98 heavy chain.

The isolation of anti-EDB antibody scFv(L19) has been described before (19). The scFv fragment specific to EDA was isolated from the human antibody library ETH-2 (19) using published procedures (20) and the recombinant protein comprising domains 11, EDA, and 12 of human fibronectin as antigen (21). The ETH-2–derived clone was used as template for the construction of an affinity maturation library, which was screened for the identification of EDA binders with improved affinity. The antibody sequence is reported in Results. The detailed experimental procedures for antibody isolation will be published elsewhere.

Specificity ELISA. The specificity of the anti-EDA scFv antibody was tested by ELISA using the recombinant antigen comprising the domains 11, EDA, and 12 of human fibronectin as well as several other fibronectin type III homology repeat domains including the EDB of fibronectin. ELISA plate wells were coated with the recombinant antigen, blocked with 2% milk powder (Rapilait) in PBS, and incubated with PBS containing 1% milk powder, 5 μg/mL purified scFv antibody, and 1 μg/mL anti-myc antibody 9E10. After incubating for 1 h and washing, bound antibody was detected with anti-mouse IgG-horseradish peroxidase conjugate (Sigma). Peroxidase activity was detected by adding BM blue POD substrate (Roche), and the reaction was stopped by the addition of H_2SO_4. The average values and the SD from three replicate wells are reported.

Histochemistry. All stainings were done on acetone-fixed cryostat sections (10 μm) of freshly frozen tissue specimens. In many cases, freshly frozen tissue sections in microarray format were obtained from BioChain.

To verify successful *in vivo* biotinylation, staining of biotinylated structures was done as described in ref. (15) using streptavidin:biotinylated alkaline phosphatase complex (Biospa), Fast-Red TR (Sigma; in the presence of 1 mmol/L Levamisole to inhibit endogenous alkaline phosphatase), and hematoxylin solution (Sigma) for counterstaining.

Immunofluorescent staining with anti-CD98 and anti-perlecan antibodies was done according to standard protocols using Alexa Fluor 546 donkey anti-goat IgG or Alexa Fluor 546 goat anti-rat IgG (Invitrogen), respectively, as secondary antibodies.

Immunohistochemical staining with scFv antibodies, carrying peptidic tags, was done as described (22).

***In vivo* targeting with near-IR fluorescence-labeled anti-EDA antibody.** Anti-EDA human antibody fragment was labeled with the commercially available near-IR fluorophore derivative Alexa Fluor 750 carboxylic acid succinimidyl ester (Invitrogen) according to the provider's protocol. The degree of labeling, estimated according to the Invitrogen labeling protocol, was five dye molecules per antibody molecule. The Alexa Fluor 750–labeled scFv fragment (in a final concentration of 0.3 mg/mL) was injected (200 μL per mouse, i.e., 60 μg antibody per mouse) in the tail vein of 129Sv mice 3 weeks after i.v. injection of mutant (18) F9 teratocarcinoma cells. Mice organs were excised 6 h after injection of the labeled antibody and imaged with a home-built IR fluorescence imager (23) equipped with a tungsten halogen lamp, excitation and emission filters specific for Alexa 750, and a monochrome CCD camera.

Quantitative biodistribution study with radioiodinated anti-EDA antibody. The *in vivo* targeting performance was evaluated quantitatively by biodistribution analysis as described previously (24). For this study, the noncovalent homodimeric antibody format ("diabody") was used, which was obtained by replacement of the linker between the variable heavy and variable light chain by a shorter linker comprising only the amino acid sequence GSSGG. In brief, the purified antibody was radioiodinated and injected into the tail vein of immunocompetent 129Sv mice bearing s.c. implanted F9 murine teratocarcinoma (7 μg, 12 μCi per mouse). Mice were sacrificed 24 h after injection, organs were weighed, and radioactivity was counted with a Packard Cobra gamma counter. Radioactivity content of representative organs was expressed as the percentage of the injected dose per gram of tissue (%ID/g).

Results

Experimental strategy. The perfusion-based chemical proteomic methodology used for the comparative analysis of accessible proteins in liver and in F9 liver metastases is depicted in Fig. 1*A*. These tumors develop large metastatic foci on the surface and inside the mouse liver (Fig. 1*B*). Under terminal anesthesia, tumor-bearing mice were perfused with 15 mL of a 1.8-mmol/L solution of sulfosuccinimidyl-6-[biotin-amido]hexanoate (1 mg/mL) in PBS (pH, 7.4), supplemented with 10% Dextran-40 as plasma expander. The procedure, which typically lasted 10 min, allowed the removal of blood from all the organs of the major circulation and the selective biotinylation of accessible proteins, both on the luminal and abluminal aspects of blood vessels. Virtually all blood vessels of F9 liver metastases were efficiently and selectively labeled with this procedure, as confirmed by histochemical staining with a streptavidin-alkaline phosphatase conjugate (Fig. 1*C, top*). In the normal liver, blood vessels were strongly stained, but labeling of some sinusoids was also detected, compatibly with the physiologic filter function of the liver (Fig. 1*C, bottom*).

The *in vivo* biotinylation was quenched by perfusion with a solution containing primary amines. Subsequently, specimens of liver metastases were excised from the liver, homogenized, and used for the recovery of biotinylated proteins in the presence of the strong detergent SDS by affinity chromatography on streptavidin resin (Fig. 1*A*). To minimize the risk of diffusion of metastatic proteins in the host liver, liver from *in vivo* biotinylated healthy mice was used for the study of the normal liver vasculature. The use of host liver from F9 tumor mice would have also been problematic because of the little residual healthy tissue and because it would have been difficult to exclude macroscopically the presence of micrometastases. In total, samples from seven *in vivo* biotinylated healthy mice and nine *in vivo* biotinylated F9 metastases-bearing mice were used for the proteomic analysis. In addition, specimens from two healthy and three metastases-bearing non-biotinylated mice were used as negative controls. Stringent washing procedures and on-resin tryptic digestion of streptavidin-captured proteins from F9 metastases and normal liver (processed in parallel) yielded a collection of peptides, which could be separated, identified, and compared using nano-HPLC and MALDI-TOF/TOF mass spectrometric procedures (16).

Identification of differentially expressed proteins and splice variants. In total, 1,291 different peptides were identified (>95% Mascot confidence level), which were grouped by the Mascot software to 497 different peptide sets (see Supplementary Table S1).

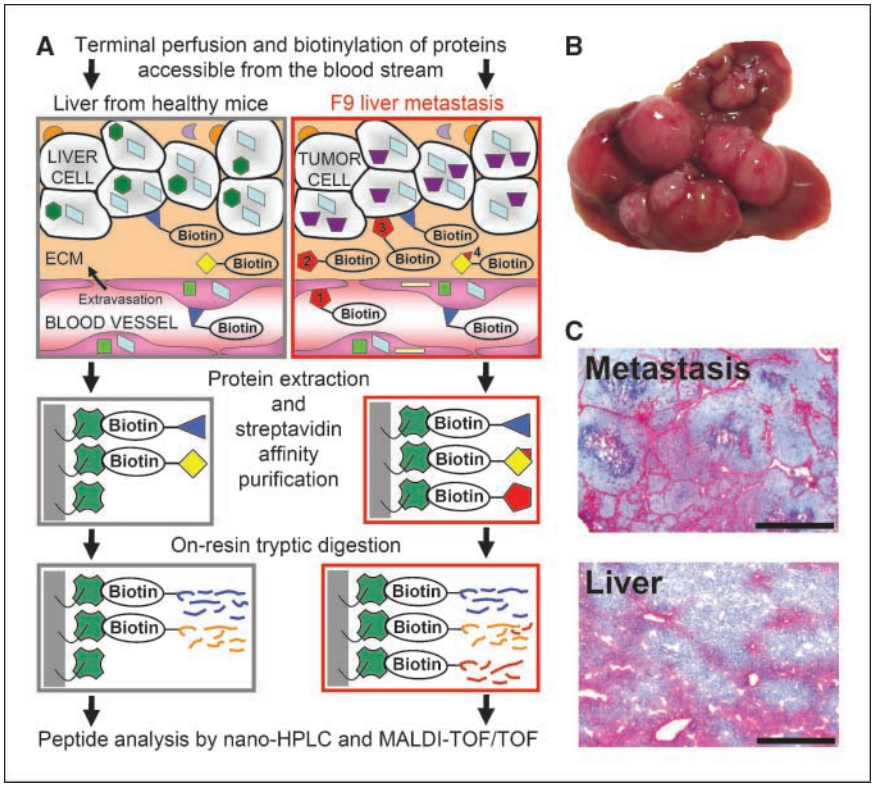

Figure 1. *In vivo* biotinylation of vascularly accessible proteins. *A,* the scheme illustrates the chemical proteomic approach for target discovery. Healthy mice or mice with F9 liver metastases were subjected to a terminal perfusion with a biotinylation reagent. This procedure led to the *in vivo* biotinylation of proteins accessible from the blood stream [e.g., (*1*) luminal membrane proteins of endothelial cells as well as (*2*) proteins in the extracellular matrix and (*3*) proteins in the plasma membranes of tumor or parenchyma cells in close proximity to the blood vessels. Subsequently, total protein extracts were prepared (using 2% SDS as detergent) of tissue specimens from the normal liver of healthy mice as well as from the metastases. From these total protein extracts, the biotinylated proteins were purified on streptavidin sepharose and digested on the resin with trypsin. The resulting peptides were separated by nano-HPLC and analyzed by MALDI-TOF/TOF mass spectrometry. Comparison of the proteins identified in the metastases with those identified in the normal liver specimens revealed candidate markers of metastases (see protein represented by red pentagon in the scheme). Furthermore, a comparison of the identified peptides could reveal (*4*) tumor-specific, alternatively spliced domains of such proteins of which other peptides were also found in the normal tissue (see protein domain represented by small red triangle attached to the yellow square). *B,* excised liver with F9 metastases, the tumor model used in this study. *C,* histochemical staining of biotinylated structures in cryosections from metastasis and normal liver tissue specimens with streptavidin-alkaline phosphatase and Fast Red showed efficient and selective biotinylation of vascular structures in the metastases. In the liver, tissue blood vessels were strongly biotinylated, but in addition, extravasation into sinusoid structures was observed as expected due to the anatomic structure of the liver. *Bars,* 500 μm.

Some of these peptide sets (62; see Supplementary Table S1) were found in negative control samples from non-biotinylated mice (like carboxylases which carry endogenous biotin as a cofactor, keratins as contaminants, or very abundant proteins like serum albumin). Of the residual 435 identified peptide sets, 331 could be annotated by the Mascot software unambiguously to a single protein, whereas 104 peptide sets were annotated to multiple (in total to 358) proteins. In most cases, multiple proteins annotated to the same peptide set belong to a related protein family (e.g., immunoglobulins) or can even be the same proteins with different database entries (see Supplementary Table S1). Of the 435 different peptide sets, 117 were exclusively found in metastasis specimens, 193 only in healthy liver specimens, and 125 in both tissue types. Table 1 lists a representative set of proteins that were found only in the healthy liver specimens, only in the F9 metastasis specimens, or in both. The number of mice in which the protein was identified is indicated. In the normal liver specimens, several intracellular enzymes were identified, possibly reflecting a rapid internalization of the sulfosuccinimidyl-6-[biotin-amido]hexanoate reagent in hepatocytes of the sinusoids. However, several membrane proteins and secreted proteins were also found, including the asialoglycoprotein receptor 1, the transmembrane proteins TIARP and carbonic anhydrase XIV. Similarly, many membrane and secreted proteins were found exclusively in the metastasis samples, including CD98 heavy chain, collagen XIV, vitronectin, clusterin, biglycan, laminin γ-1 chain, and endoglin. Many of the proteins identified in the liver metastases had previously been reported to be associated with angiogenesis (see Discussion).

Whenever proteins were found both in the liver and metastasis specimens (e.g., fibronectin, fibrinogen, perlecan), it could happen that the proteins were present at substantially different levels in the two samples. If this was the case, this should be reflected in the number of specimens in which the proteins were detected (Table 1) and/or in the number of peptides (as well as normalized peptide signal intensity; ref. 17) observed in the liver and metastasis samples. Supplementary Table S2 lists some prominent examples, in which more peptides were found in the tumor specimens compared with normal liver. For instance, 38 tryptic peptides from fibronectin were found only in metastases, whereas 1 peptide was found only in normal liver. A total of 11 peptides were found in both types of specimens. Similarly, a clear abundance of identified peptides in the metastases was observed for proteins such as fibrin/fibrinogen, albumin, and serotransferrin (additionally, α2-macroglobulin and murinoglobulin-1 were identified in all tumor samples but not in normal liver, see Table 1), consistent with the notion that blood coagulation may provide a provisional stroma in which metastatic cells attach and grow (25).

The striking abundance of fibronectin-derived peptides detected in liver metastases, in spite of the fact that liver is the site of fibronectin biosynthesis, prompted us to investigate differences in the relative abundance of fibronectin-derived peptides and the overexpression of alternatively spliced domains. Supplementary Table S3 lists all fibronectin peptides identified in the proteomic analysis. Figure 2*A* shows a graphical representation of the fibronectin sequence and domain structure and the location of the peptides identified in the tumor and/or in the normal liver. Mouse fibronectin contains two type III globular extra-domains, which may undergo alternative splicing: EDA and EDB (for a review, see ref. 26). In addition, the IIICS segment (variable region, V region) undergoes different splicing patterns in humans (for a review, see ref. 27) and mice (see, e.g., ref. 28). Interestingly, all three EDA-derived peptides as well as the IIICS-derived peptide identified in our proteomic analysis were observed only in the tumor samples. EDB-derived peptides would not be visible in this analysis due to the fact that EDB contains no lysine residue and the two arginines give rise to peptides that are too large in size for detection. Figure 2*B* shows the relative intensity of normalized MS signals for two fibronectin-derived peptides: IAWESPQGQVSR, which is located within the EDA domain, and FLTTTPNSLLVSWQAPR, which is located in the fibronectin type III domain 16. The latter peptide was more abundant in the metastasis specimens, but was clearly detectable also in the normal liver counterpart. By contrast, EDA-derived peptides gave strong signals in the metastasis samples, but were completely undetectable (i.e., >100-fold lower signal) in normal liver.

Immunofluorescence. Figure 3 shows immunohistochemical findings that support the expression data described in the previous section. We studied the expression and localization of perlecan and CD98 heavy chain: two of the proteins that had been found in virtually all tumor specimens with excellent liver:metastasis discrimination (Table 1). Antibodies to CD98 heavy chain strongly stain the membrane of tumor cells (Fig. 3*A*), including those that are adjacent to the neovasculature in liver metastases (see Discussion). By contrast, perlecan was preferentially observed around vascular structures both in liver and in F9 tumor metastases, with a clear overexpression in the metastatic foci (Fig. 3*B*).

Validation of EDA as a marker for antibody-based tumor targeting. We generated a human monoclonal antibody specific to the EDA of fibronectin from a large human antibody library available in the lab (29). The amino acid sequence of the anti-EDA scFv antibody fragment is shown in Fig. 4*A*. Specificity of the antibody was assessed by ELISA (Fig. 4*B*). It is important to note that the antibody did not cross-react with the EDB of fibronectin.

A striking discrimination between liver structures and metastatic neovasculature was observed for the EDA and EDB domains of fibronectin. In both cases, a strong and specific staining of the metastatic blood vessels was observed, whereas normal liver and virtually all normal organs (exception made for the endometrium in the proliferative phase and some vessels of the ovaries) scored negative in this immunohistochemical analysis (Fig. 4*C*).

To test the usefulness of EDA as a target for ligand-based vascular targeting of metastases, we did *in vivo* targeting experiments using near-IR fluorescence imaging. The human anti-EDA antibody fragment in the scFv format was labeled with Alexa Fluor 750 and injected i.v. into F9 metastases-bearing mice. Near-IR fluorescence imaging of the excised organs revealed a striking accumulation of the targeting agent in the metastatic lesions (Fig. 4*D*). For the quantitative assessment of the tumor-targeting properties of the anti-EDA antibody, a biodistribution analysis in 129Sv mice bearing s.c. F9 tumors was done using i.v. injection of a radioiodinated preparation of the noncovalent homodimeric form (diabody) of the antibody. Uptake values after 24 h (average % injected dose per gram tissue ± SD from an experiment with four replicate mice) showed a striking accumulation of the anti-EDA antibody in the tumor (13.0 ± 5.5% ID/g), but only low values in normal organs (e.g., 0.8 ± 0.06% ID/g in the liver, 1.2 ± 0.08% ID/g in the lung, 1.8 ± 0.4% ID/g in the spleen, 0.6 ± 0.08% ID/g in the heart, 1.9 ± 0.2% ID/g in the kidney, 1.1 ± 0.2% ID/g in the intestine, and 1.2 ± 0.3% ID/g in the blood).

Finally, we tested the expression of EDA in human tissues by immunohistochemical analysis using the human anti-EDA antibody (Fig. 5). Importantly, EDA was found to be strongly expressed in the neovasculature of human lung metastases and liver metastases as well as of a large panel of different other human tumors, whereas

expression in normal tissues was negligible. Furthermore, a comprehensive study of human lung tumors showed that EDA is abundantly expressed in all important subtypes of lung cancer (see Supplementary Fig. S1).

Discussion

The *in vivo* biotinylation of accessible proteins in the vascular structures of healthy liver and liver metastases of F9 tumors, followed by a comparative mass spectrometric analysis, has led to the identification of qualitative and quantitative differences at the molecular level. These observations extend prior transcriptomic studies of tumor neovasculature, which have thus far mainly concentrated on endothelial cells and on primary tumors, rather than on metastasis (e.g., refs. 8, 9).

The identification of protein markers (such as CD98) on the surface of perivascular tumor cells is not surprising. Several antibody-based tumor-targeting studies have revealed that

Table 1. Selection of proteins identified only in metastasis, only in liver, or in both types of tissue specimens

Accession number	Protein name	Liver (total = 6)*	Metastasis (total = 8)*
Q8R0Y6	10-Formyltetrahydrofolate dehydrogenase	5	0
P49429	4-hydroxyphenylpyruvate dioxygenase	5	0
Q61176	Arginase 1	5	0
P16015	Carbonic anhydrase III	5	0
Q9WVT6	Carbonic anhydrase XIV	5	0
P24270	Catalase	5	0
P00186	Cytochrome P450 1A2	5	0
Q8VCW9	Cytochrome P450, family 2, subfamily a, polypeptide 12	5	0
Q64374	Regucalcin	5	0
Q6XL44	UDP glycosyltransferase 1 family polypeptide	5	0
Q62452	UDP-glucuronosyltransferase 1-7	5	0
P25688	Uricase	5	0
Q91W31	Transmembrane protein TIARP	4	0
P34927	Asialoglycoprotein receptor 1	3	0
P70694	Estradiol 17β-dehydrogenase 5	5	4
P24549	Retinal dehydrogenase 1	5	4
Q9QXZ6	Solute carrier organic anion transporter	5	7
P11087	Collagen α1(I) chain	5	8
Q921I1	Serotransferrin	5	8
Q63880	Liver carboxylesterase 31	4	1
Q9JJL3	Solute carrier organic anion transporter family member 1B2	4	3
Q01279	Epidermal growth factor receptor	4	6
P11276 †	Fibronectin	4	8
Q99K47	Fibrinogen, α polypeptide	2	8
O88322	Nidogen-2	1	7
Q8K0E8	Fibrinogen β chain	1	8
Q05793	Perlecan	1	8
Q61838	α-2-Macroglobulin	0	8
Q80X19	Collagen α 1(XIV) chain	0	8
P28665	Murinoglobulin-1	0	8
Q06890	Clusterin	0	7
Q60849	CD98 heavy chain	0	6
P29788	Vitronectin	0	5
O08677	Kininogen-1	0	4
P20918	Plasminogen	0	4
Q61247	α-2-Antiplasmin	0	3
Q01339	β-2-Glycoprotein I	0	3
P28653	Biglycan	0	3
P21995	Embigin	0	3
P02468	Laminin γ-1 chain	0	2
Q8BKG3	Tyrosine-protein kinase-like 7	0	2
Q8K100	Endoglin	0	1

*Numbers indicate in how many of the six healthy *in vivo* biotinylated mice or the eight metastases-bearing *in vivo* biotinylated mice the protein was identified in the corresponding tissue samples. See Supplementary Table S1 for a list of all identified proteins in these *in vivo* biotinylated samples and additional negative control samples from unperfused mice.

† The results for fibronectin precursor P11276 include also peptides that were originally assigned by the Mascot software to the fibronectin database entries Q3UHL6 and Q3TCF1 but also match with the entry P11276.

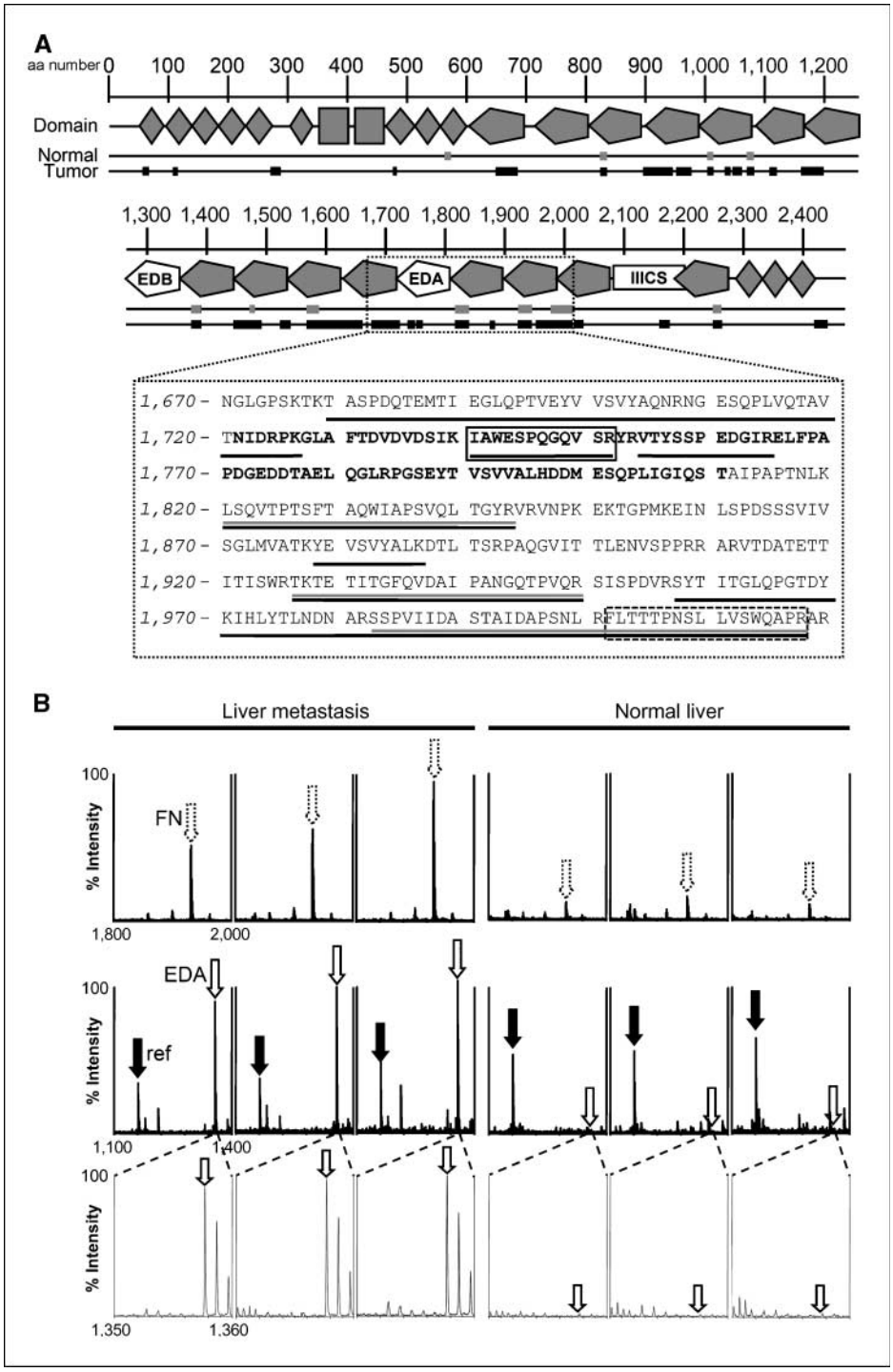

Figure 2. Mass spectrometric identification of the EDA of fibronectin specifically in the metastases. *A,* schematic representation of the mouse fibronectin domain structure with amino acid numbers. Different domain types: *diamond,* fibronectin type I; *rectangle,* fibronectin type II; *pentagon,* fibronectin type III domain. *Gray or black rectangles,* identified peptides (normal healthy liver or F9 metastasis, respectively) below the domain structure at the corresponding amino acid sequence position. The EDA and EDB, as well as the IIICS stretch of the fibronectin sequence, are indicated. *One-letter code,* sequence portion from position 1,670 to 2,010. *Underlined sequence portions,* identified peptides (color codes as described above). The ion peaks of the two framed peptides were used to detect the absence or presence of the EDA (peptide with solid line frame) and of the constant region of fibronectin (peptide with dashed line frame) as shown in *B*. *B,* mass spectra of two selected HPLC fractions (*top* and *middle*, respectively) are shown for three replicate samples of liver metastasis (*left*) and three replicate samples of healthy normal liver samples (*right*). The ion peak heights are normalized to the internal standard (see Supplementary Experimental Procedures) and, thus, allow a semiquantitative comparison of the corresponding peptide in the different samples. *Top, white arrow with dashed line border,* peptide FLTTTPNSLLVSWQAPR (*FN*), which is derived from a constant region of fibronectin. The ion peak of this peptide is stronger in the metastasis samples, but is also present in the normal liver samples, indicating that the fibronectin molecule is, in principle, present in both types of tissues, but seems to be more highly abundant in the metastasis. *Middle, white arrow with solid line border,* peptide IAWESPQGQVSR (*EDA*), which is derived from the alternatively spliced EDA of fibronectin. The EDA peptide is only detectable in metastasis samples. *Black arrow,* reference peptide (*ref*) used to identify the HPLC fraction in which the EDA peptide elutes. *Bottom,* close-up view of the mass spectra at the position of the EDA peptide ion peak proving the absence of this peptide in normal liver.

perivascular tumor cells are rapidly accessible to i.v. administered labeled antibody fragments (30, 31). Other proteins, such as perlecan and fibronectin isoforms, display an expression pattern that is closely associated to vascular structures. In particular, fibronectin isoforms seem to be ideally suited for ligand-based vascular tumor-targeting applications, in light of their specific and abundant expression in the neovasculature of both primary and metastatic lesions.

Some of the proteins found to be overexpressed in tumor liver metastases (Table 1 and Supplementary Table S2) have been considered before for antibody-based vascular targeting applications. For instance, endoglin has long been known to be overexpressed in the tumor neovasculature (see, e.g., ref. 6), although its expression in normal organs is not negligible (32).

Interestingly, β-2-glycoprotein 1 (Table 1) has recently been described as the antigen of the antibody 3G4 (33), which targets anionic phospholipids on tumor blood vessels. A chimeric version of 3G4 (tarvacin/bavituximab) is currently in clinical development for oncological applications (Peregrine Pharmaceuticals, Inc.).

In our proteomic analysis, we found the CD98 heavy chain only in the metastasis but not in normal liver. Interestingly, CD98 heavy chain has been shown to mediate integrin-dependent signals, which promote tumorigenesis (34). In a recent transcriptomic study, CD98 heavy chain has been suggested as a marker of poor prognosis and as a potential therapeutic target in breast cancer (35).

Another protein which we found up-regulated in metastases is perlecan (identified in eight out of eight metastasis specimens with a total of 10 different peptides but only in one out of six healthy liver specimens with only one peptide; see Table 1 and Supplementary Table S2). Perlecan is a large multi-domain extracellular matrix proteoglycan that plays a crucial role in tissue and organ development (for an overview, see ref. 36). Perlecan has been shown to be overexpressed around newly formed blood vessels in a variety of human cancers, including tumors of the breast (37), liver (38), and ovarian (39), as well as colon and prostate (40).

Some of the most abundant proteins found to be closely associated to liver metastases of F9 tumors are blood components and/or products of blood coagulation. It has long been known that blood coagulation leads to the formation of a provisional stroma, which is instructive and permissive for the attachment and growth of metastatic cells (25).

Our findings confirm the value of unbiased chemical proteomics methodologies (such as the one described in this article,

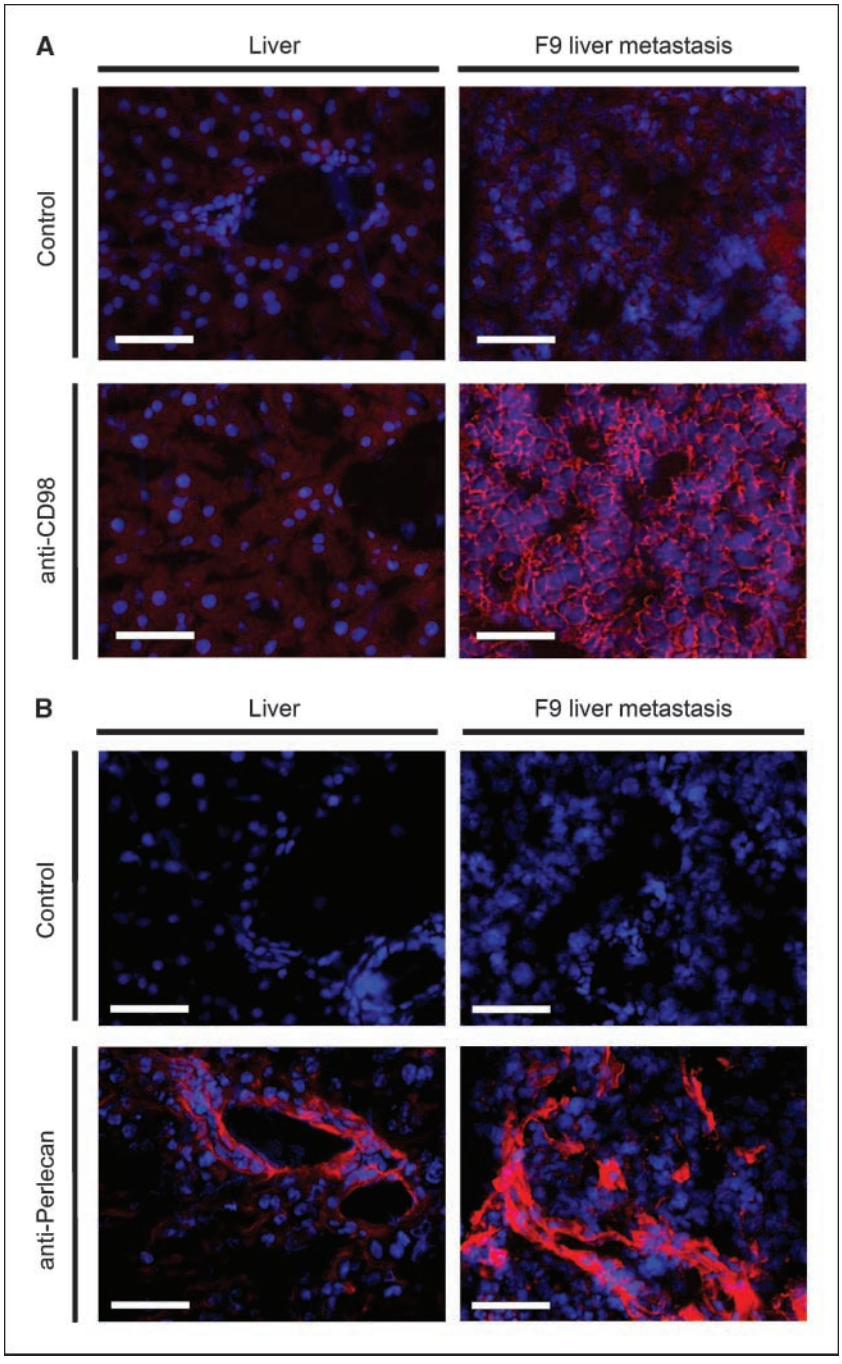

Figure 3. Target validation by immunohistochemistry. Staining of cryo-sections from normal mouse liver and F9 liver metastases with antibodies specific to CD98 heavy chain (*A*) or to perlecan (*B*). In line with the proteomic results (see Table 1), CD98 heavy chain was exclusively detected in the membrane of tumor cells (including tumor cells adjacent to blood vessels), and perlecan was observed around vascular structures of both tissue types, but with a clear overexpression in the metastases. *Bars,* 50 μm.

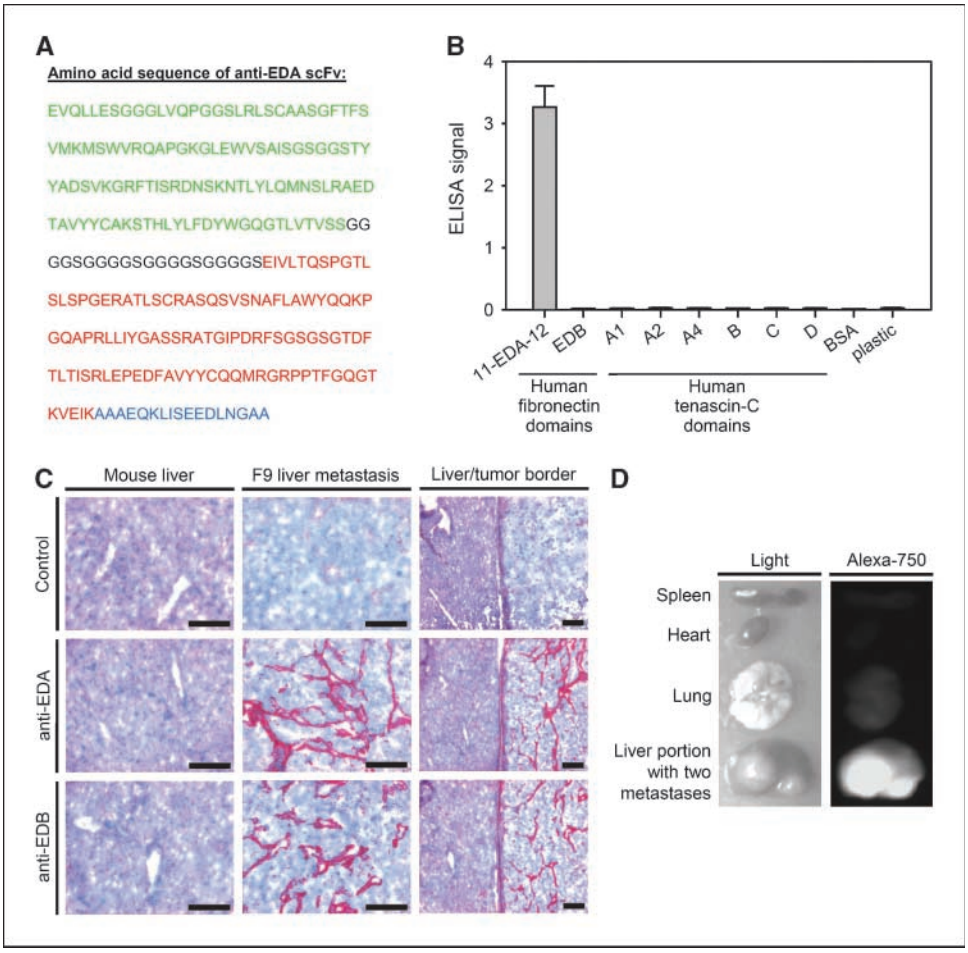

Figure 4. Validation of EDA as an antigen for antibody-based vascular targeting of metastases. *A,* amino acid sequence (shown in the one-letter amino acid code according to standard IUPAC nomenclature) of the anti-EDA antibody fragment in scFv format, comprising the variable heavy-chain (*green letters*) and the variable light-chain (*red letters*) domains, connected via a linker (*black letters*), as well as a COOH-terminal peptidic tag (*blue letters*) containing the c-myc epitope sequence EQKLISEEDL. *B,* a specificity ELISA proved specific binding of the anti-EDA antibody to the fibronectin stretch comprising domains 11, EDA, and 12 (the recombinant antigen used for antibody isolation), whereas no binding was detectable toward EDB or other related fibronectin type III repeat domains, such as certain domains of tenascin-C. *C,* immunohistochemical staining of F9 liver metastases and adjacent normal mouse liver tissue with the anti-EDA antibody revealed a strong vascular pattern of staining in the metastases, whereas no specific staining was detectable in adjacent liver tissue. In the negative controls, the scFv was omitted. The staining pattern is similar to the staining pattern of the scFv(L19) flag, which recognizes the fibronectin EDB, a well-established marker of neovascular structures. *Bars,* 100 μm. *D,* the anti-EDA antibody was labeled with the near-IR fluorescence dye Alexa-750 and injected into live mice bearing F9 liver metastases. Six hours after injection of the labeled antibody, mice were sacrificed, and organs were excised and imaged with a near-IR fluorescence imager. Although normal liver and other organs showed only background fluorescence, metastases were strongly positive, indicating a successful *in vivo* targeting of the antibody-fluorophore conjugate to the metastatic lesions. For further results of quantitative biodistribution studies using radioiodinated anti-EDA antibody, see text.

which relies on the biotinylation of primary amino groups in accessible proteins) for the characterization of a comprehensive list of proteins, which are selectively and abundantly found in the organs or in the sites of the pathology of interest. An atlas of abundant and accessible markers of pathology will be invaluable for ranking different tumor-associated antigens, which may be considered for antibody-based vascular targeting applications.

The alternatively spliced EDA domain of fibronectin was chosen for further characterization as a vascular marker of primary tumors and of metastatic lesions, for many reasons. First, we had observed a striking discrimination between tumor and normal liver specimens for EDA in our proteomic analysis. Second, unlike other candidate markers (such as α-2-macroglobulin, collagen α1 or murinoglobulin-1), EDA was known to be absent in serum and most normal tissues. Third, our lab has done more than 10 years of research on a different splice isoform of fibronectin, and we were most excited to see EDA(+) fibronectin ranking among the most promising vascular markers of neovasculature in metastatic lesions.

The immunohistochemical discrimination between liver metastases and host organ, using antibodies directed against the EDA and EDB domains of fibronectin, is impressive, particularly if one considers that the liver is the main site of plasma fibronectin synthesis. Even more importantly, our near-IR fluorescence imaging experiments showed that an anti-EDA antibody is capable of selectively targeting metastases *in vivo*. In our quantitative biodistribution experiments using mice bearing s.c. F9 tumors, the anti-EDA antibody in diabody format reached excellent tumor-to-blood (10.8:1) and tumor-to-organ ratios (>6.8:1). Furthermore, our immunohistochemical validation of EDA expression in human tissues revealed a strong staining of vascular structures in a large panel of human metastases and primary tumors, whereas expression in normal human tissues was negligible. Among others,

we found EDA to be abundantly expressed in all important subtypes of lung cancer, the most common cancer in the world today (see Supplementary Fig. S1).

Antibodies represent the fastest growing sector of pharmaceutical biotechnology. Most of the antibodies in clinical developments are being investigated in the cancer field. Our group has moved L19-based biopharmaceuticals to phase II clinical trials for the therapy of cancer, making EDB one of the best characterized markers of angiogenesis in terms of biodistribution studies in tumor-bearing animals with radiolabeled antibody preparations (24, 41–43), of imaging studies in patients with cancer (13), and of therapeutic antibody derivatives (for a recent review, see ref. 7). The findings presented in this article suggest that EDA may represent an equally attractive target for the antibody-based delivery of bioactive agents to the neovasculature not only of solid tumors, but also of metastatic lesions. To the best of our

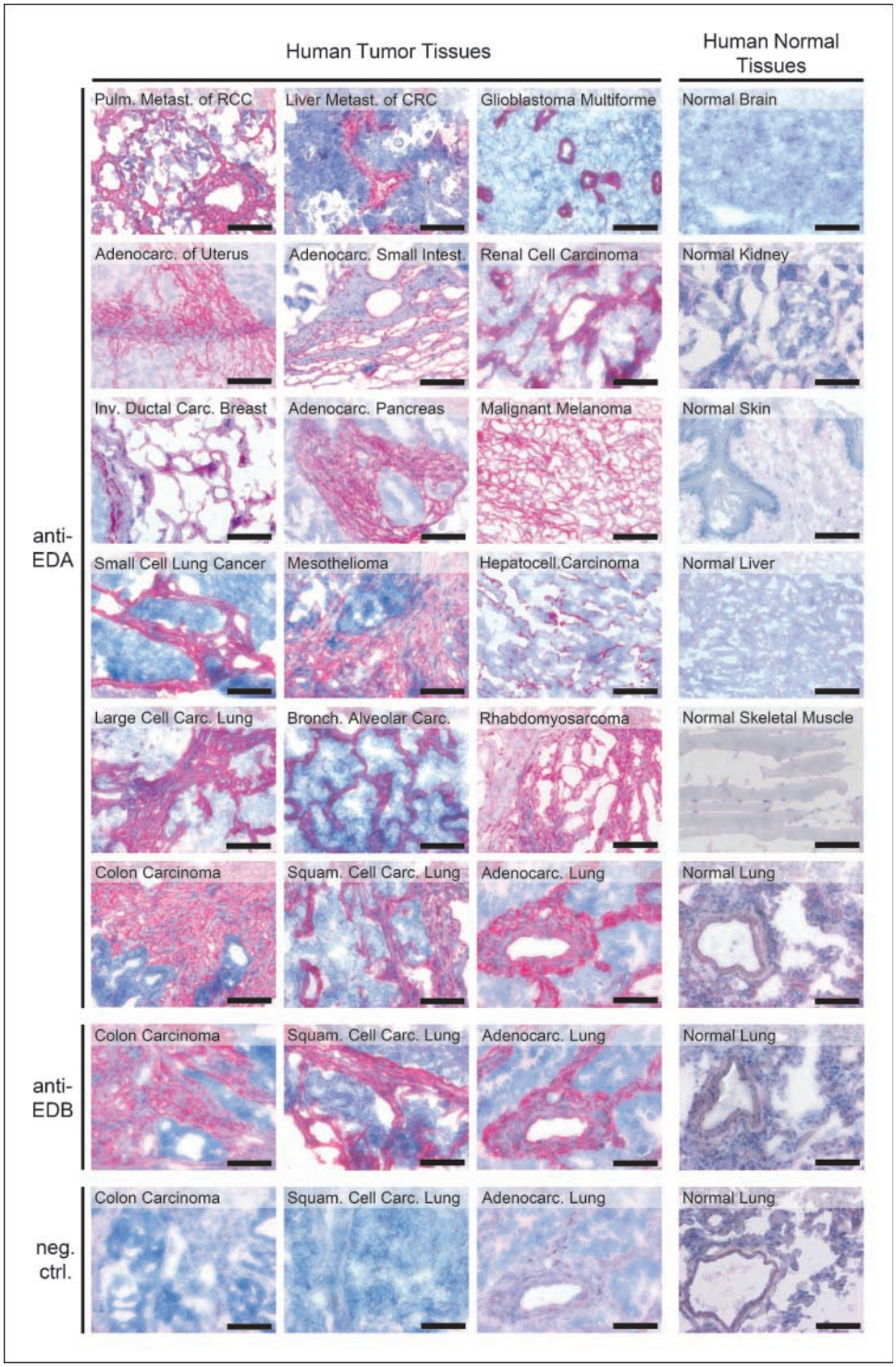

Figure 5. Expression of EDA in human metastases and primary tumors. The human antibody fragment specific to EDA was used to assess antigen expression in a large panel of human metastatic lesions and primary tumors by immunohistochemistry. Virtually all human tumors tested were strongly positive for EDA, whereas no or only a weak background staining was observed in human normal tissue sections with the anti-EDA antibody. No positive staining was detectable in negative controls omitting the scFv antibody. The staining pattern in tumors was mainly vascular and was similar to the staining pattern of scFv(L19), which recognizes the fibronectin EDB, a well-established marker of neovascular structures. Furthermore, a comprehensive immunohistochemical study on human lung tumor sections showed that EDA is abundantly expressed in all important subtypes of lung cancer (see Supplementary Fig. S1). *RCC,* renal cell carcinoma; *CRC,* colorectal carcinoma. *Bars,* 100 μm.

knowledge, anti-EDA antibodies have not yet been tested in imaging or biodistribution studies and not in the clinic. Furthermore, whereas there are reports about EDA expression in tumor cells and in solid tumors at the mRNA level (see, e.g., refs. 44, 45), at the level of isolated protein (46) and at the immunohistochemical level (21, 47–50), we could not find any report of EDA expression in the neovasculature of liver and lung metastases. The work presented in this article strongly encourages the clinical development of anti-EDA antibody derivatives, in full analogy to anti-EDB antibodies.

Acknowledgments

Received 4/18/2007; revised 8/10/2007; accepted 9/19/2007.

Grant support: Swiss National Science Foundation, the Gebert-Ruef Foundation, the Schweizer Krebsliga, the ETH Zurich, and the European Union projects Selective targeting of angiogenesis and tumor stroma, Selective fluorinated inhibitors of matrix metallo-proteinases III and IX, and Immunophotodynamic therapy.

The costs of publication of this article were defrayed in part by the payment of page charges. This article must therefore be hereby marked *advertisement* in accordance with 18 U.S.C. Section 1734 solely to indicate this fact.

We thank the Functional Genomics Center Zurich for access to instrumentation and technical support. We are grateful to Prof. Dr. Luciano Zardi for help in the immunohistochemistry analysis of human liver metastases.

References

1. Hanahan D, Weinberg RA. The hallmarks of cancer. Cell 2000;100:57–70.
2. Carter PJ. Potent antibody therapeutics by design. Nat Rev Immunol 2006;6:343–57.
3. Adams GP, Weiner LM. Monoclonal antibody therapy of cancer. Nat Biotechnol 2005;23:1147–57.
4. Schrama D, Reisfeld RA, Becker JC. Antibody targeted drugs as cancer therapeutics. Nat Rev Drug Discov 2006; 5:147–59.
5. Neri D, Bicknell R. Tumour vascular targeting. Nat Rev Cancer 2005;5:436–46.
6. Thorpe PE. Vascular targeting agents as cancer therapeutics. Clin Cancer Res 2004;10:415–27.
7. Rybak JN, Trachsel E, Scheuermann J, Neri D. Ligand-based vascular targeting of disease. Chem Med Chem 2007;2:22–40.
8. St Croix B, Rago C, Velculescu V, et al. Genes expressed in human tumor endothelium. Science 2000; 289:1197–202.
9. Huminiecki L, Bicknell R. *In silico* cloning of novel endothelial-specific genes. Genome Res 2000; 10:1796–806.
10. Ran S, Downes A, Thorpe PE. Increased exposure of anionic phospholipids on the surface of tumor blood vessels. Cancer Res 2002;62:6132–40.
11. Oh P, Li Y, Yu J, et al. Subtractive proteomic mapping of the endothelial surface in lung and solid tumours for tissue-specific therapy. Nature 2004;429:629–35.
12. Castronovo V, Waltregny D, Kischel P, et al. A chemical proteomics approach for the identification of accessible antigens expressed in human kidney cancer. Mol Cell Proteomics 2006;5:2083–91.
13. Santimaria M, Moscatelli G, Viale GL, et al. Immunoscintigraphic detection of the ED-B domain of fibronectin, a marker of angiogenesis, in patients with cancer. Clin Cancer Res 2003;9:571–9.
14. Menrad A, Menssen HD. ED-B fibronectin as a target for antibody-based cancer treatments. Expert Opin Ther Targets 2005;9:491–500.
15. Rybak JN, Ettorre A, Kaissling B, Giavazzi R, Neri D, Elia G. *In vivo* protein biotinylation for identification of organ-specific antigens accessible from the vasculature. Nat Methods 2005;2:291–8.
16. Roesli C, Neri D, Rybak JN. *In vivo* protein biotinylation and sample preparation for the proteomic identification of organ- and disease-specific antigens accessible from the vasculature. Nature Protocols 2006; 1:192–9.
17. Scheurer SB, Rybak J-N, Roesli C, et al. Identification and relative quantification of membrane proteins by surface biotinylation and two-dimensional peptide mapping. Proteomics 2005;5:2718–28.
18. Terrana B, Rusciano D, Pacenti L. Organ colonization pattern of retinoic acid-treated and -untreated mouse embryonal carcinoma F9 cells. Cancer Res 1987;47: 3791–7.
19. Pini A, Viti F, Santucci A, et al. Design and use of a phage display library. Human antibodies with subnanomolar affinity against a marker of angiogenesis eluted from a two-dimensional gel. J Biol Chem 1998;273: 21769–76.
20. Giovannoni L, Viti F, Zardi L, Neri D. Isolation of anti-angiogenesis antibodies from a large combinatorial repertoire by colony filter screening. Nucleic Acids Res 2001;29:E27.
21. Borsi L, Castellani P, Allemanni G, Neri D, Zardi L. Preparation of phage antibodies to the ED-A domain of human fibronectin. Exp Cell Res 1998;240:244–51.
22. Brack SS, Silacci M, Birchler M, Neri D. Tumor-targeting properties of novel antibodies specific to the large isoform of tenascin-C. Clin Cancer Res 2006;12: 3200–8.
23. Birchler M, Neri G, Tarli L, Halin C, Viti F, Neri D. Infrared photodetection for the *in vivo* localisation of phage-derived antibodies directed against angiogenic markers. J Immunol Methods 1999;231:239–48.
24. Berndorff D, Borkowski S, Moosmayer D, et al. Imaging of tumor angiogenesis using Tc-99m–labeled human recombinant Anti–ED-B fibronectin antibody fragments. Journal of nuclear medicine 2006;47:1707–16.
25. Dvorak HF. Tumors: wounds that do not heal. Similarities between tumor stroma generation and wound healing. N Engl J Med 1986;315:1650–9.
26. Kaspar M, Zardi L, Neri D. Fibronectin as target for tumor therapy. Int J Cancer 2006;118:1331–9.
27. ffrench-Constant C. Alternative splicing of fibronectin—many different proteins but few different functions. Exp Cell Res 1995;221:261–71.
28. Bergijk EC, Baelde HJ, Kootstra CJ, De Heer E, Killen PD, Bruijn JA. Cloning of the mouse fibronectin V-region and variation of its splicing pattern in experimental immune complex glomerulonephritis. J Pathol 1996;178: 462–8.
29. Silacci M, Brack S, Schirru G, et al. Design, construction, and characterization of a large synthetic human antibody phage display library. Proteomics 2005; 5:2340–50.
30. Adams GP, Schier R, McCall AM, et al. High affinity restricts the localization and tumor penetration of single-chain fv antibody molecules. Cancer Res 2001;61: 4750–5.
31. Niesner U, Halin C, Lozzi L, et al. Quantitation of the tumor-targeting properties of antibody fragments conjugated to cell-permeating HIV-1 TAT peptides. Bioconjug Chem 2002;13:729–36.
32. Balza E, Castellani P, Zijlstra A, Neri D, Zardi L, Siri A. Lack of specificity of endoglin expression for tumor blood vessels. Int J Cancer 2001;94:579–85.
33. Luster TA, He J, Huang X, et al. Plasma protein β-2-glycoprotein 1 mediates interaction between the anti-tumor monoclonal antibody 3G4 and anionic phospholipids on endothelial cells. J Biol Chem 2006;281:29863–71.
34. Feral CC, Nishiya N, Fenczik CA, Stuhlmann H, Slepak M, Ginsberg MH. CD98hc (SLC3A2) mediates integrin signaling. Proc Natl Acad Sci U S A 2005;102:355–60.
35. Esseghir S, Reis-Filho JS, Kennedy A, et al. Identification of transmembrane proteins as potential prognostic markers and therapeutic targets in breast cancer by a screen for signal sequence encoding transcripts. J Pathol 2006;210:420–30.
36. Knox SM, Whitelock JM. Perlecan: how does one molecule do so many things? Cell Mol Life Sci 2006;63: 2435–45.
37. Guelstein VI, Tchypysheva TA, Ermilova VD, Ljubimov AV. Myoepithelial and basement membrane antigens in benign and malignant human breast tumors. Int J Cancer 1993;53:269–77.
38. Roskams T, De Vos R, David G, Van Damme B, Desmet V. Heparan sulphate proteoglycan expression in human primary liver tumours. J Pathol 1998;185:290–7.
39. Gonzalez EM, Mongiat M, Slater SJ, Baffa R, Iozzo RV. A novel interaction between perlecan protein core and progranulin: potential effects on tumor growth. J Biol Chem 2003;278:38113–6.
40. Iozzo RV. Perlecan: a gem of a proteoglycan. Matrix Biol 1994;14:203–8.
41. Viti F, Tarli L, Giovannoni L, Zardi L, Neri D. Increased binding affinity and valence of recombinant antibody fragments lead to improved targeting of tumoral angiogenesis. Cancer Res 1999;59:347–52.
42. Borsi L, Balza E, Bestagno M, et al. Selective targeting of tumoral vasculature: comparison of different formats of an antibody (L19) to the ED-B domain of fibronectin. Int J Cancer 2002;102:75–85.
43. Berndorff D, Borkowski S, Sieger S, et al. Radioimmunotherapy of solid tumors by targeting extra domain B fibronectin: identification of the best-suited radioimmunoconjugate. Clin Cancer Res 2005;11:7053–63s.
44. Oyama F, Hirohashi S, Shimosato Y, Titani K, Sekiguchi K. Deregulation of alternative splicing of fibronectin pre-mRNA in malignant human liver tumors. J Biol Chem 1989;264:10331–4.
45. Matsumoto E, Yoshida T, Kawarada Y, Sakakura T. Expression of fibronectin isoforms in human breast tissue: production of extra domain A+/extra domain B+ by cancer cells and extra domain A+ by stromal cells. Jpn J Cancer Res 1999;90:320–5.
46. Borsi L, Carnemolla B, Castellani P, et al. Monoclonal antibodies in the analysis of fibronectin isoforms generated by alternative splicing of mRNA precursors in normal and transformed human cells. J Cell Biol 1987; 104:595–600.
47. Scarpino S, Stoppacciaro A, Pellegrini C, et al. Expression of EDA/EDB isoforms of fibronectin in papillary carcinoma of the thyroid. J Pathol 1999;188: 163–7.
48. Koukoulis GK, Shen J, Virtanen I, Gould VE. Immunolocalization of cellular fibronectins in the normal liver, cirrhosis, and hepatocellular carcinoma. Ultrastruct Pathol 1995;19:37–43.
49. Lohi J, Tani T, Laitinen L, Kangas L, Lehto VP, Virtanen I. Tenascin and fibronectin isoforms in human renal cell carcinomas, renal cell carcinoma cell lines and xenografts in nude mice. Int J Cancer 1995; 63:442–9.
50. Heikinheimo K, Morgan PR, Happonen RP, Stenman G, Virtanen I. Distribution of extracellular matrix proteins in odontogenic tumours and developing teeth. Virchows Arch B Cell Pathol Incl Mol Pathol 1991;61: 101–9.